



# Enhanced visible-light photocatalytic oxidative desulfurization of model fuel over Pt-decorated carbon-doped TiO<sub>2</sub> nanoparticles

Abdollah Ostovar<sup>1</sup> · Afsanehsadat Larimi<sup>2</sup> · Zhi Jiang<sup>3</sup> · Marzieh Lotfi<sup>4</sup> · Cyrus Ghotbi<sup>1</sup> · Farhad Khorasheh<sup>1</sup>

Received: 2 September 2022 / Accepted: 17 March 2023 / Published online: 23 March 2023  
© The Author(s), under exclusive licence to Springer-Verlag GmbH Germany, part of Springer Nature 2023

## Abstract

Modification of photocatalysts to improve their adsorption and photocatalytic activity in the oxidative desulfurization of liquid fuels has been reported by many investigators. In this study, Pt-decorated carbon-doped TiO<sub>2</sub> nanoparticles were synthesized by hydrothermal and photo-deposition techniques and were subsequently used in photocatalytic oxidative desulfurization of dibenzothiophene (DBT) in *n*-heptane as a simulated liquid fuel with methanol as the extracting solvent. Carbon-doped TiO<sub>2</sub> was first synthesized by a simple self-doping method. Pt was then loaded by a photo-deposition technique. The synthesized photocatalysts (labeled as YPt-CT where Y is percent Pt loading) were characterized by X-ray diffraction (XRD), photoluminescence (PL), field emission scanning electron microscopy (FESEM), N<sub>2</sub>-physisorption, UV-Vis diffusive reflectance spectra (UV-Vis DRS), transmission electron microscopy (TEM), Fourier transform infrared spectra (FTIR), and nitrogen sorption measurements. The removal efficiency of DBT was 98% in the presence of 2 g/l of 0.5Pt-CT catalyst under visible-light irradiation ( $\lambda > 400$  nm), ambient pressure, and reaction temperature of 40°C.

**Keywords** Oxidative desulfurization · Photooxidative degradation · Photocatalysis · Titanium dioxide · Visible-light active · First-order reaction

## Introduction

Combustion of fuels containing various sulfur species including mercaptans, sulfides, and thiophenes by moving and stationary sources can lead to significant formation of SO<sub>x</sub> that is of serious environmental concern (Pillai et al. 2012; Song 2003). Various processes including catalytic hydrodesulfurization (HDS) (Shang et al. 2020),

adsorption (Song et al. 2017), and oxidative desulfurization (ODS) (Zhang et al. 2013, 2017) can be used for sulfur removal from liquid fuels. HDS is the most common method used in refineries to reduce the sulfur content (Boonyasuwat & Tscheikuna 2017; Shang et al. 2020). HDS processes, however, require severe process conditions as well as significant hydrogen consumption in the presence of a catalyst. Alternative desulfurization approach, among them oxidative desulfurization, have therefore received considerable attentions due to the mild conditions they employ as well as their cost effectiveness (Song 2003). Photocatalysts have attracted great attentions to promote many reactions (Tayyab et al. 2022) (Liu et al. 2021) (Tayyab et al. 2022) (Danish et al. 2021) (Chamack et al. 2022) (Moradi et al. 2020) (Nematollahi et al. 2020) (Larimi et al. 2022) (Chi et al. 2022) including ODS given their low cost, good stability, and reusability. In photocatalytic ODS, light irradiation would generate electrons and holes that lead to the formation of highly active radicals that would oxidize the sulfur compounds to the corresponding sulfones (Huang et al. 2020; Li et al. 2016; Yaghoot-Nezhad et al. 2020). The highly polar

Responsible Editor: Sami Rtimi

✉ Afsanehsadat Larimi  
alarimi@nri.ac.ir

- <sup>1</sup> Department of Chemical and Petroleum Engineering, Sharif University of Technology, Tehran, Iran
- <sup>2</sup> Department of Chemical and Process Engineering, Niroo Research Institute, Tehran, Iran
- <sup>3</sup> Research Center for Combustion and Environmental Technology, Shanghai Jiao Tong University, Shanghai 200240, China
- <sup>4</sup> Department of Chemical Engineering, Jundi-Shapur University of Technology, Dezful, Iran

sulfones can be removed by extraction (Anpo et al. 2009; Kalantari et al. 2016; Masoomi et al. 2015).

Non-metal doping is an effective strategy to reduce the energy band gap of titanium dioxide TiO<sub>2</sub> (Abdollahi et al. 2022). Non-metal dopants including N (Nasirian Bachelor 2021), S (McManamon et al. 2015), B (Giannakas et al. 2016), and F (Samsudin et al. 2016) have been successfully used to enhance the photocatalytic activity by limiting electron-hole recombination and narrowing the band gap. Carbon doping of TiO<sub>2</sub> would enhance the light absorption and expand it into the visible light by generating a new energy level in the band gap. It would also result in enhanced adsorption of reactants by providing greater catalyst surface site density. In a recent self-doped method, TiO<sub>2</sub>-N-C photocatalysts were prepared by passing N<sub>2</sub> and CO over Ti at 450–550°C to form thin films that showed superior efficiency in self-reduction under visible light (Choi et al. 2006). C-doped anatase TiO<sub>2</sub> was also synthesized by a sol gel method that showed enhanced photocatalytic efficiency under visible light irradiation ( $\lambda > 400$  nm) (Liu et al. 2014). Carbon self-doped TiO<sub>2</sub> was also recently synthesized by a hydrothermal technique for remediation of acid orange that showed superior activity as compared with C-doped TiO<sub>2</sub> prepared by the sol gel method (Ochoa Rodríguez et al. 2019).

Doping with metals such as Ni (Nematollahi et al. 2021), Cu (Hitam et al. 2016), Fe (Kalantari et al. 2017), Pt (Larimi & Khorasheh 2020), Bi (Nematollahi et al. 2019), and Ag (Jaafar et al. 2015) have enhanced the sensitivity of TiO<sub>2</sub> to irradiation in the visible region, thereby promoting the photocatalytic activity. These metals, however, can intensify the production of charge carriers by acting as active sites. Platinum (Pt) has been widely investigated as a promoter for photocatalytic activity (Liu et al. 2021) (Moradi et al. 2019). Bi-doped TiO<sub>2</sub> was decorated with Pt nanoparticles and showed enhanced activity in the photo-reduction of CO<sub>2</sub> due to the desirable effect of Pt for electron trapping (Moradi et al. 2020). The enhanced photodegradation activity of Pt/TiO<sub>2</sub> was shown to be mainly due to the oxidized Pt species and not the metallic nanoparticles of Pt (Shu et al. 2020). Pt-N-TiO<sub>2</sub> nanomaterials were also synthesized to investigate their performance in benzoic acid photo-oxidation with N-doped TiO<sub>2</sub> having a higher visible-light absorbance than pure TiO<sub>2</sub> while additional Pt loading by a sol gel impregnation method significantly enhanced the life of holes and positively influenced the photo induced electrons (Giannakas et al. 2017).

To the best of our knowledge, there has not been a published report on simultaneous modification of TiO<sub>2</sub>-based photocatalysts with Pt metal loading and C non-metal doping for oxidative desulfurization of liquid fuels. Herein, we have investigated both non-metal doping of TiO<sub>2</sub> and metal decorating for photocatalytic oxidative desulfurization. First, carbon-doped TiO<sub>2</sub> was prepared using a self-doped method followed by Pt loading by a photo-deposition technique.

## Materials and methods

### Materials

Titanium *n*-butoxide (Ti (O*Bu*)<sub>4</sub>, 98%), nitric acid (>65%), dibenzothiophene (DBT), methanol (absolute, >98%), and *n*-heptane were purchased from Sigma-Aldrich and ethanol (absolute, >96%) from Golriz company in Iran. All materials were used without further treatments.

### Synthesis

#### Synthesis of carbon-doped TiO<sub>2</sub>

Carbon-doped TiO<sub>2</sub> was prepared by a method reported in the literature (Ochoa Rodríguez et al. 2019). Solution A was first prepared by dissolving 6 ml of Ti(O*Bu*)<sub>4</sub> in 20 ml of ethanol. Solution B was prepared by mixing 0.4 ml of nitric acid, 17 ml of ethanol, and 1.6 ml of water. Both solutions were stirred for 30 min at room temperature and then mixed and stirred for an additional 30 min. The resulting mixture was left in a dark place at ambient conditions for 48 h and was subsequently placed in a Teflon-lined autoclave reactor for hydrothermal treatment for 10 h under self-generated pressure at 180°C. The resulting white solid was separated by filtration and dried at 60°C and subsequently calcined at three different temperatures of 200, 400, and 600°C and were designated as CT200, CT400, and CT600, respectively.

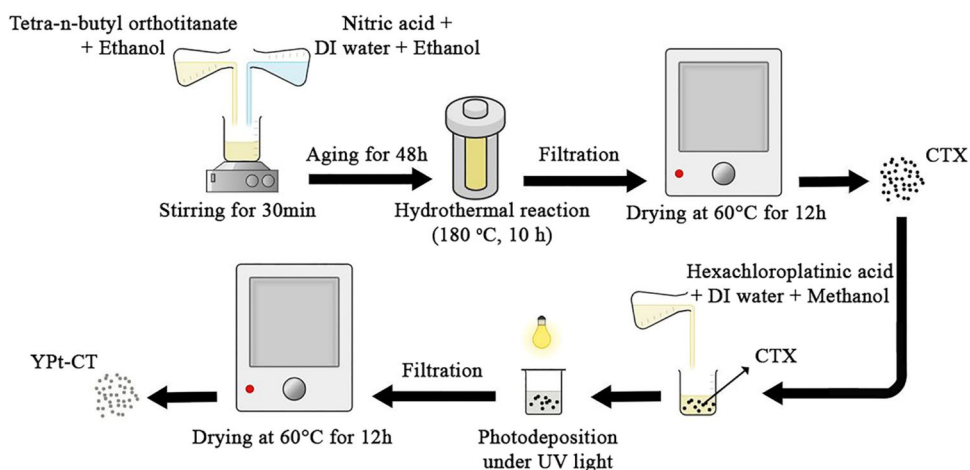
#### Photo-deposition of platinum on carbon-doped TiO<sub>2</sub>

Three Pt-loaded samples containing 0.5%, 1%, and 2% (by mass) of Pt were synthesized by a photo-deposition method. An aqueous solution of 20 vol% methanol was used to suspend 0.25 g of carbon-doped TiO<sub>2</sub> into a 100-ml quartz cell and the required amount of 4 g per liter of H<sub>2</sub>PtCl<sub>6</sub> solution was then added to the cell. Prior to illumination, inert N<sub>2</sub> gas was purged into the cell to remove dissolved oxygen so to prevent Pt from oxidation. After 4 h of UV irradiation by a 250 W Hg lamp, the gray-colored precipitate was collected using a filter paper. The adsorbed ions on surface of the collected solid were then removed by washing with distilled water several times. The sample was then dried at 90°C for 12 h. The samples were designated as YPt-CT where Y is the mass percent of Pt. The entire synthesis process is illustrated in Fig. 1.

### Characterization

A D8 Advance (Bruker AXS, Germany) diffractometer was used to obtain the X-ray diffraction (XRD)

**Fig. 1** Synthesis procedure of photocatalysts



patterns of the powder samples with Cu K $\alpha$  radiation ( $k = 1.5406 \text{ \AA}$ ) and using an X-ray radiation source at 40 kV and 40 mA. FTIR spectroscopy was performed by ABB Bomem model MB100 spectrometer in 500–4000  $\text{cm}^{-1}$  wavenumber range. Field emission scanning electron microscopy (FESEM) images and energy dispersive X-ray spectroscopy (EDX) were recorded using MIRA TESCAN microscope with 15 kV operating voltage. UV-vis spectrophotometer (Shimadzu UV-2550) was used to obtain diffuse reflectance spectra (DRS) with KBr taken as reference in wavelength range of 300–800 nm. A F6500 fluorescence photometer equipped with an excitation wavelength of 300 nm was used to obtain photoluminescence (PL) spectra at room temperature. TF20 Jeol 2100F field emission transmission electron microscope was used to acquire transmission electron microscopy (TEM) images. Nitrogen adsorption–desorption at 77 K was obtained by a Belsorp mini II equipment to determine the Brunauer-Emmett-Teller (BET) surface area,

Barrett–Joyner–Halenda (BJH) pore size distribution, and the total pore volume. Fourier transform infrared spectra (FTIR) were obtained using a Thermo Nicolet IR 100 FTIR spectrometer in the wavelength range of 900–4000  $\text{cm}^{-1}$ .

### Photocatalytic desulfurization

The sulfur containing model fuel was prepared by dissolving 17.5 mg of dibenzothiophene in 35 ml of *n*-heptane and 35 ml of methanol as extraction solvent. The solution was added to a two-necked glass reactor. One hundred and forty milligrams of photocatalyst were subsequently added to the reactor under constant stirring. The irradiation source was a 250 W sodium vapor lamp which could have resulted in a temperature rise during the reaction. A cooling system was implemented to maintain the reactor temperature at about 40 °C. The reactor content was kept under dark for 60 min to establish adsorption/desorption equilibrium prior to the irradiation source to be turned on.

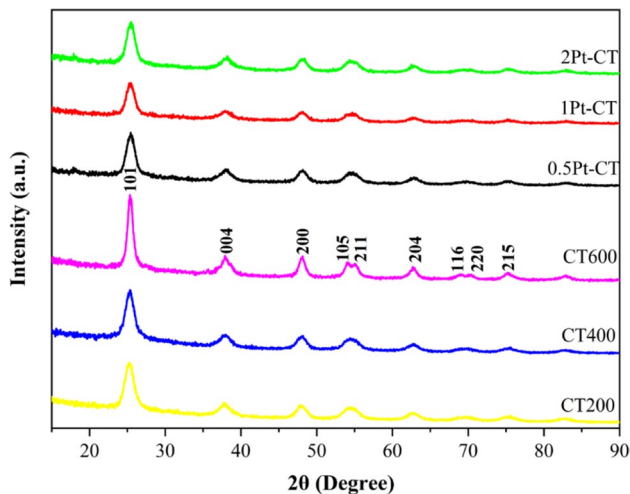


**Fig. 2** XRD patterns of samples

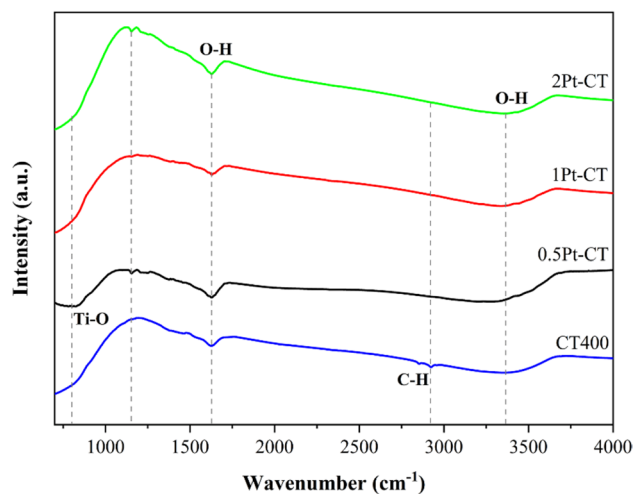


**Fig. 3** FTIR spectra of photocatalyst samples

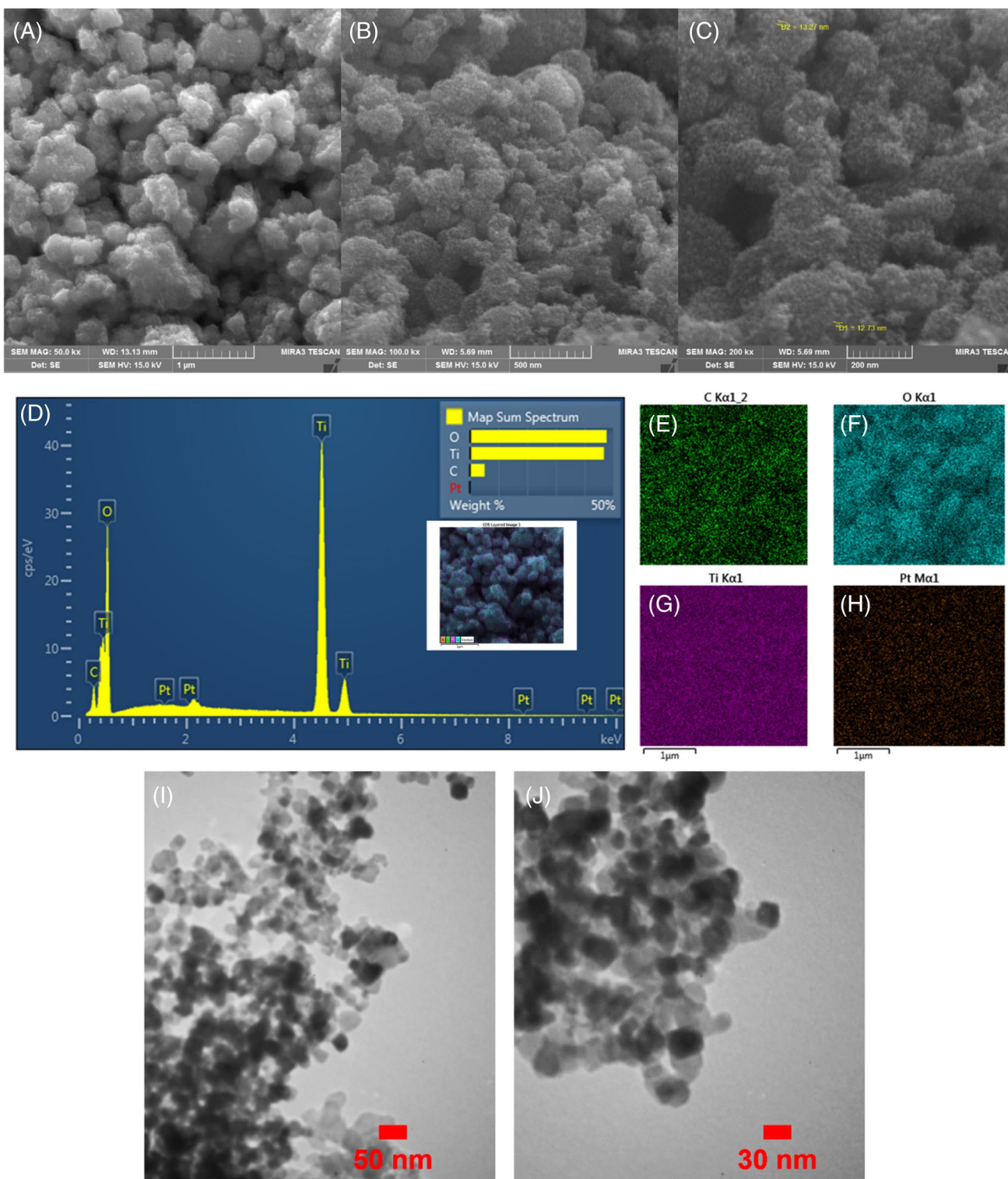


**Fig. 4** (A, B, C) FESEM images, (D) EDX spectrum, (E, F, G, H) images of elemental mapping, and (I, J) TEM images of 0.5Pt-CT

During the experiment, samples were regularly taken from the reactor and were subsequently filtered and analyzed. A UV-visible spectrophotometer was used to measure the

absorbance at 470 nm to determine the DBT concentration for each sample. DBT removal efficiency was calculated using the following equation:

**Table 1** Weight and mole percentages of different elements in 0.5Pt-CT sample

Element	Weight %	Mole %
C	5.19	9.84
O	47.7	67.88
Ti	46.8	22.2
Pt	0.31	0.04
Total	100	100

$$\text{Efficiency} = \frac{C_0 - C}{C_0} \quad (\text{Eq. 1})$$

where  $C_0$  and  $C$  are DBT concentrations initially and at any time,  $t$ , respectively. All reported data were mean values of  $\geq 3$  experiments and the calculated DBT removal efficiency had an accuracy of  $\pm 2\%$  due to analytical error.

## Results and discussion

### Characterization of photocatalysts

#### XRD

In order to explore the crystal structure synthesized photocatalysts, the XRD patterns were obtained and are presented in Fig. 2. Anatase peaks were observed at  $2\theta$  values of 25.5, 37.9, 48.1, 53.6, 54.7, 62.2, 68.9, 70.1, and 74.8° in all the patterns that corresponded to the characteristic planes (101), (004), (200), (105), (211), (204), (116), (220), and (215), respectively (Moradi et al. 2018; Ochoa Rodríguez et al. 2019). There were no peaks associated with the rutile phase. An increase in the calcination temperature led to an increase in the crystallinity of CT samples. Crystallinity, however, decreased when Pt was present. The crystal sizes for each sample were calculated from Scherrer equation and are presented in Table 2, indicating that the crystals became larger with increasing Pt content.

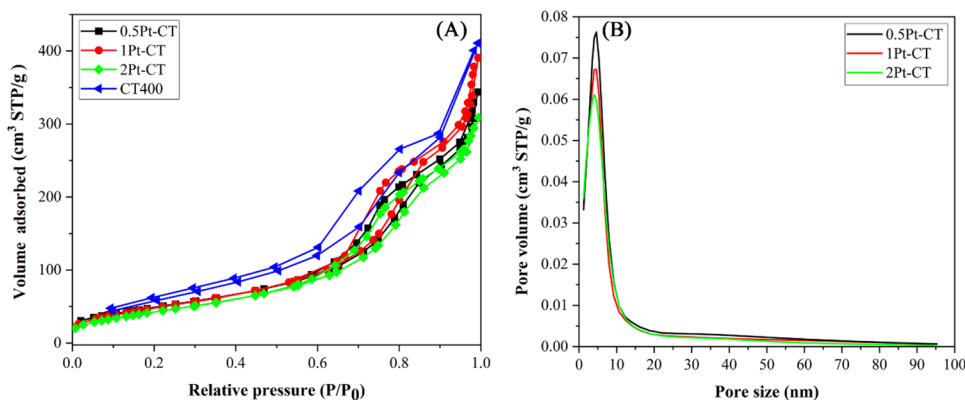
#### FTIR

Figure 3 presents the FTIR spectra for TC400 and YPt-CT samples in the wavelength range of 500 to 4000  $\text{cm}^{-1}$ . A broad band was observed in all spectra between 800 and 400  $\text{cm}^{-1}$  that was associated with the vibrations of the Ti-O bonds in the anatase phase of  $\text{TiO}_2$  (Peng et al. 2017). The peaks at 1638 and 3374  $\text{cm}^{-1}$  were associated with the vibratory stretching and bending of O-H, respectively (Huang et al. 2009). Reactive oxygen species are created when the surface hydroxyl groups interact with photo-generated holes and inhibit the recombination of photo generation charges (Liu et al. 2012).  $\text{TiO}_2$ -OH bonds on the surface are often believed to originate from an exothermic reaction occurring during the preparation process (Huang et al. 2008). A weak peak seen at 2923  $\text{cm}^{-1}$  on the TC400 sample that could be attributed to the stretching vibrations of  $-\text{CH}_3$  (Erdem et al. 2001). The YPt-CT samples appeared to be free of organic species on their surface based on the fact that no peaks were observed to coincide with  $-\text{CH}_3$ ,  $-\text{CH}_2$ , or  $-\text{CH}$  bonds.

#### FESEM, EDX, and TEM

To shed light on the morphological properties of the photocatalysts, FESEM and TEM analyses were performed. The FESEM images for 0.5Pt-CT photocatalyst are shown in Fig. 4(A–C) for different magnifications. Particles were spherical and dispersed in a narrow size range with high homogeneity. The sample was observed to be uniformly shaped with an average diameter of 10 nm.

It may not be a completely superficial method, but EDX has an advantage of a quick surface analysis (Ochoa Rodríguez et al. 2019). The EDX spectrum and the mapping of the associated elemental distributions are illustrated in Figs. 4(D) and 4(E–H), respectively. The metallic elements titanium and platinum, unlike oxygen and carbon, have multiple peaks in the energy diffraction spectrum, which can be due to the ionization of these elements with different

**Fig. 5** (A)  $\text{N}_2$  adsorption–desorption isotherms of samples and (B) BJH pore size distributions of samples

**Table 2** Structural properties of the synthesized photocatalysts

Samples	$S_{\text{BET}}$ (m <sup>2</sup> /g)	Total pore volume (cm <sup>3</sup> /g)	Pore diameter (nm)	Crystal size (nm)
CT400	230	0.635	11.05	6.3
0.5Pt-CT	175.7	0.521	11.86	7.3
1Pt-CT	174	0.587	13.5	7.4
2Pt-CT	156.3	0.467	11.95	7.4

electrical charges. Pt constituted to approximately 0.5% of the weight of the catalyst which was different from 0.31% that was obtained at the surface of catalyst. As indicated in Table 1, the molar ratio of O to Ti was approximately 3. EDX analysis has shown that Ti-O bonds were highly concentrated at the surface. Ti and O displayed similar profiles indicating that the elements were dispersed and Pt also displayed uniform dispersion within TiO<sub>2</sub> structure (Peng et al. 2017).

The TEM images for 0.5Pt-CT sample at 30- and 50-nm scales are presented in Fig. 4(J, J) in which the dark patches are Pt particles dispersed over the carbon-doped TiO<sub>2</sub> nanoparticles that are spherical in shape. Excessive Pt doping could lead to an increase in the catalyst particle size (Ishibai et al. 2007).

### N<sub>2</sub>-physorption analysis

N<sub>2</sub> adsorption and desorption isotherms were obtained for the synthesized photocatalysts in order to investigate their specific surface area and pore size distribution and the results are presented in Fig. 5(A) and Table 2. A typical mesoporous structure was observed for all samples that were type IV according to the (International Union of Pure and Applied Chemistry) IUPAC classification (Xie et al. 2010). According to Table 2, CT400 had the largest specific surface area. Loading with Pt led to an increase in crystalline size, thereby

resulting in a decrease in surface area and total pore volume for samples containing Pt. N<sub>2</sub> isotherms also showed a narrow hysteresis loop due to the mesoporous structure of the samples (Li et al. 2014). Figure 5(B) shows the BJH pore size distributions indicating that the majority of pores had diameters ranging from 1 to 10 nm. There was a peak (at about 4.61 nm pore size) for all Pt samples that diminished with increasing Pt content in accordance with the TEM and XRD results.

### UV-vis DRS analysis

UV-vis DRS analysis were performed to reveal the optical properties of photocatalysts. The UV-vis diffuse reflectance spectra of synthesized samples are shown in Fig. 6(A). An extrinsic dopant into the lattice will alter the absorption band of a photocatalyst (Mousavi-Kamazani & Ashrafi 2020). In comparison with other samples, the 0.5Pt-CT sample had a greatest absorption rate of visible light (beyond 400 nm) as indicated in Fig. 6(B). The DRS spectra also indicated that the 1Pt-CT had lower absorption compared with both the 2Pt-CT and CT400 samples. The bands gap energies were estimated from DRS spectra using the Kubelka-Munk equation as shown in Fig. 6(B) where the intercepts of the asymptotes to the plots of  $(\alpha h\nu)^{1/2}$  versus photon energy (eV) were used to estimate the band gap energies as reported in Table 3.

### PL

Photoluminescence (PL) spectroscopy was performed to investigate the recombination of charge carriers associated with the structure of synthesized samples (Dong et al. 2011; Moradi, Khorasheh, & Larimi 2020). A comparison of the PL spectra at room temperature is presented in Fig. 7. All PL signals had a broad peak located at or near 580 nm in the visible range that may be due to the traps on the surface or to their band gap (Stevanovic et al. 2011). TC400 had

**Fig. 6** (A) UV-vis DRS spectra of samples and (B) Tauc plots of samples

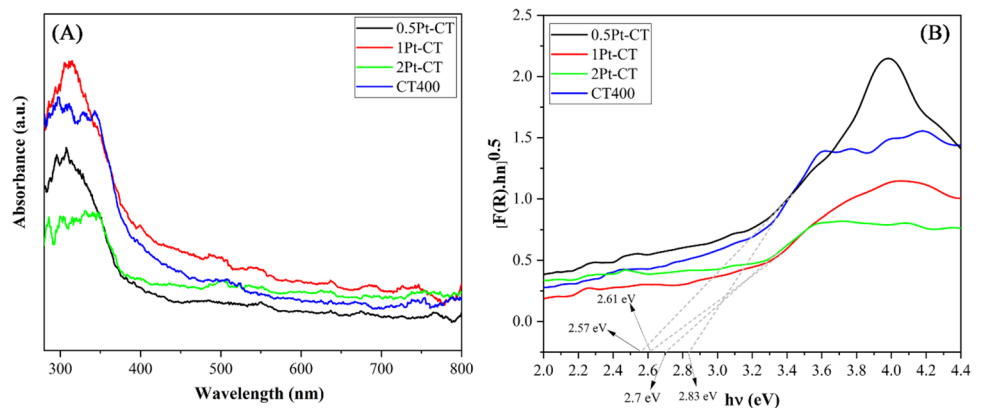


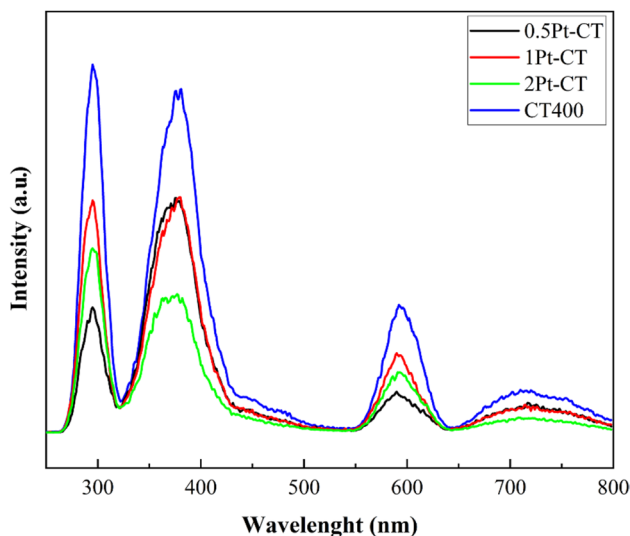
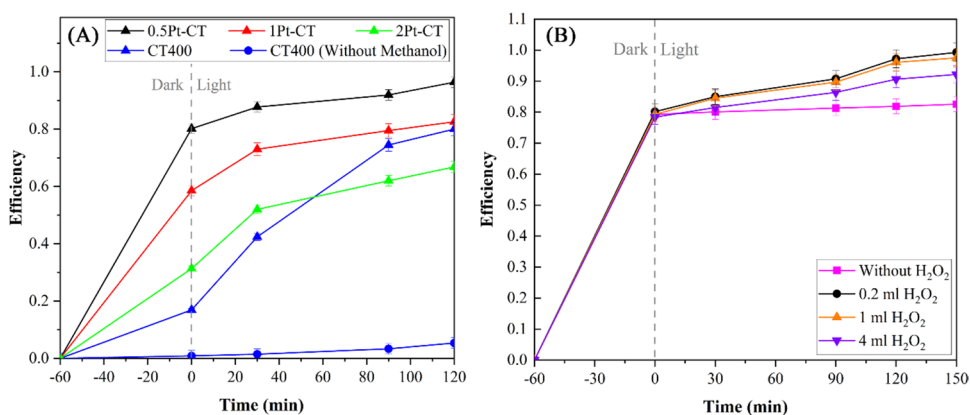
**Table 3** Band gap energy of samples

Sample	Band gap (eV)
0.5Pt-CT	2.57
1Pt-CT	2.61
2Pt-CT	2.7
CT400	2.83

the highest intensity compared with other samples indicating significantly more recombination of electron/hole and subsequently lower photocatalytic activity.

### Photocatalytic activity

The results of photocatalytic oxidative desulfurization of a dibenzothiophene (DBT) containing solution in *n*-heptane as a model fuel over Pt-CT samples with varying amounts of Pt under visible-light conditions are presented in Fig. 8(A). The photodegradation processes occurred after the adsorption of

**Fig. 7** Photoluminescence spectra of prepared photocatalysts**Fig. 8** (A) Photocatalytic oxidative desulfurization of DBT over different photocatalyst samples and (B) photocatalytic activity of 0.5Pt-CT with different amounts of  $H_2O_2$  oxidant

DBT on the catalyst had reached an equilibrium in the dark. The concentration of DBT remaining in the solution after the 60-min dark period indicated a significant adsorptive capacity of the catalyst for DBT that was attributed to the adsorption of electron pairs of the sulfur atoms of DBT on the vacancies of catalyst (Pham et al. 2020). The extent of DBT removal in the presence of CT400 as catalyst was only 8.1% and when methanol was added as a polar solvent it reached 83%. In the absence of methanol, the photocatalyst formed a precipitate. The products from photocatalytic oxidative desulfurization of DBT are the corresponding sulfones that can be isolated by solvent extraction (Attar & Corcoran 1978). Due to a change in polarity of sulfone compounds upon oxidation of DBT, they are easily separated from hydrocarbon fuels (Campos-Martin et al. 2010; Ismagilov et al. 2015). Photocatalytic activity increased significantly when Pt was loaded onto CT400 with DBT removal reaching its maximum of 98% with Pt loading of 0.5% that was in accordance with the DRS results that demonstrated this catalyst had the highest light absorption as well as the lowest band gap energy (2.58 eV).

Figure 8(B) demonstrates the effect of  $H_2O_2$  concentration on photocatalyst efficiency. The oxidation of DBT can be facilitated by  $H_2O_2$  oxidant combining with electrons/holes to form OH species (Li et al. 2017). Nevertheless, the presence of excess  $H_2O_2$  interferes with the degradative process due to the scavenging of oxidative species (Moradi et al. 2015). As shown in Fig. 8(B), photo-oxidation activity was very low in the absence of oxidant. With the addition of 0.2 ml of  $H_2O_2$  to the reaction mixture, DBT removal increased from 80 to 98%. Any further addition of  $H_2O_2$ , however, reduced the DBT removal efficiency.

Both photocatalytic and adsorption activity were enhanced by doping of carbon (Table 4). The optimum activity was achieved with Pt loading of 0.5%. Total DBT removal decreased with increasing Pt content beyond this optimum amount as indicated by lower light absorption for the for the 1% and 2% Pt samples as indicated by DRS

**Table 4** Comparison of adsorption and total efficiency of photocatalysts

Sample	Adsorption%	Total degradation%
CT400	16.9	83
0.5Pt-CT	80.2	99.3
1Pt-CT	58.5	87.5
2Pt-CT	31.3	66.6

results. The higher Pt content also led to a reaction solution that was darker thus resulting in a decreased light infiltrating.

DBT degradation could be described as a pseudo first-order reaction represented by Eq. 2 in terms of illumination time (Pham et al. 2020):

$$-\ln\left(\frac{C}{C_0}\right) = kt \tag{Eq. 2}$$

where  $C$  and  $C_0$  are the DBT concentrations (mg/l) at time  $t$  (h) and the initial concentration at the start of irradiation, respectively, and  $k$  is the reaction rate constant ( $\text{h}^{-1}$ ). As shown in Fig. 9, first-order kinetics was found to adequately describe DBT oxidation. 0.5Pt-CT sample had the highest rate constant of  $1.04 \text{ h}^{-1}$  followed by CT400, 1Pt-CT, and 2Pt-CT samples with corresponding rate constants of 0.69, 0.47, and  $0.37 \text{ h}^{-1}$ , respectively. The 1% Pt sample had a better efficiency as compared with TiOC-400 which may be due to presence of more active sites from Pt loading resulting in improved adsorption of DBT. CT400, on the other hand, had better photocatalytic activity as the reaction mixture for 1Pt-CT sample was darker resulting in decreased infiltration of light.

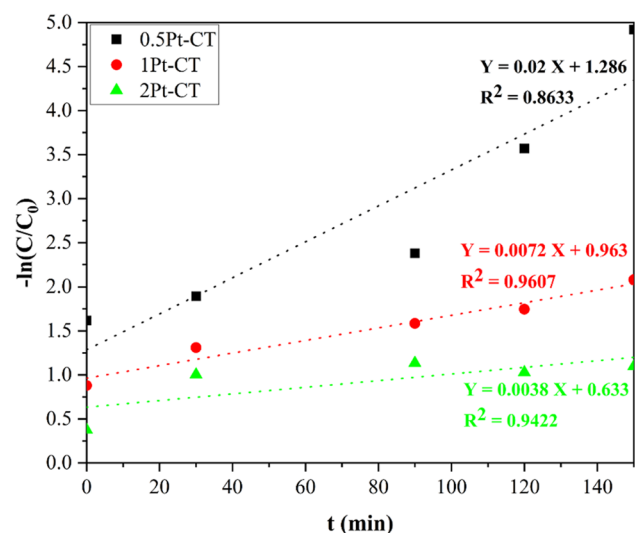


**Fig. 9** Plots for pseudo first-order kinetics for DBT removal for different photocatalysts

The C modification is believed to be critical for the visible-light photocatalysis because it introduces defects in the lattice (Yu et al. 2011) and  $\text{H}_2\text{O}_2$  has been used to elevate photocatalytic activity in the photocatalytic oxidative desulfurization experiments (Wang et al. 2014). The mechanism presented by Eqs. 3–6 can be proposed for photocatalytic oxidative desulfurization of DBT. During the absorption of photons, electrons and holes are generated respectively in the valence band (VB) and conduction band (CB) of  $\text{TiO}_2$ . A new series of energy states can be generated along the band gap of  $\text{TiO}_2$  in order to enhance photocatalytic activity through introduction of carbon as dopant in  $\text{TiO}_2$  lattice (Lin et al. 2013). According to the DRS spectra, 0.5Pt-CT sample had a lower band gap energy compared with CT400, indicating that a new state of energy had been formed after Pt loading (Li & Li 2002). Electrons generated with radiant energy in the conduction band will decompose  $\text{H}_2\text{O}_2$  to hydroxyl and hydroxyl radical. Photo-generated electrons in the semiconductor also transfer to the Pt sites where the same decomposition occurs. The hydroxyl groups in the solution react with the  $\text{h}^+$  in the VB and generate hydroxyl radicals and thus more hydroxyl radicals are produced. The degradation of DBT to  $\text{DBTO}_2$  is typically influenced by strong oxidation by  $\bullet\text{OH}$  species (Sood et al. 2015) (Wang et al. 2011). Figure 10 presents the schematic illustration of photocatalytic oxidation of model fuel over Pt-decorated carbon-doped  $\text{TiO}_2$  nanoparticles.

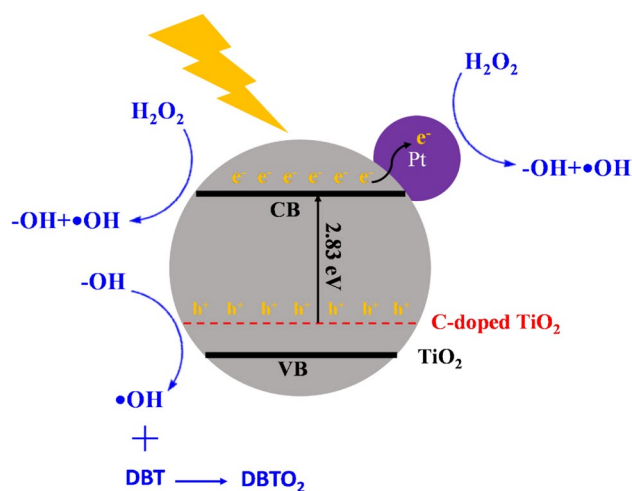
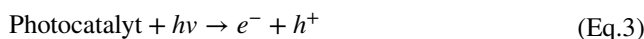


**Fig. 10** Schematic illustration of photocatalytic oxidation of model fuel over Pt-decorated carbon-doped  $\text{TiO}_2$  nanoparticles



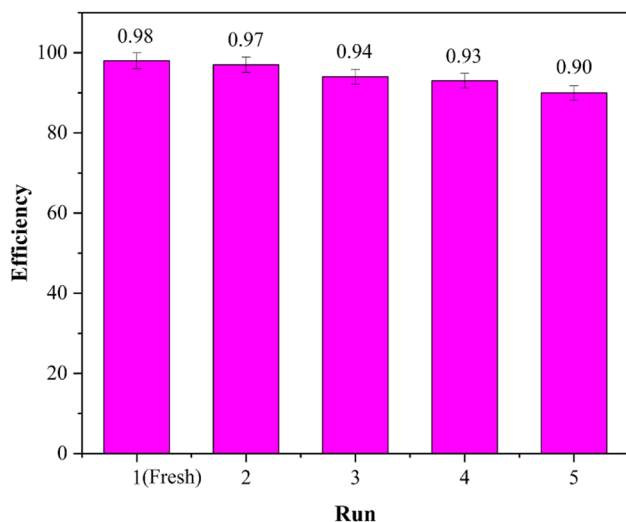


**Fig. 11** DBT removal efficiency for consecutive reaction cycles over 0.5Pt-CT sample

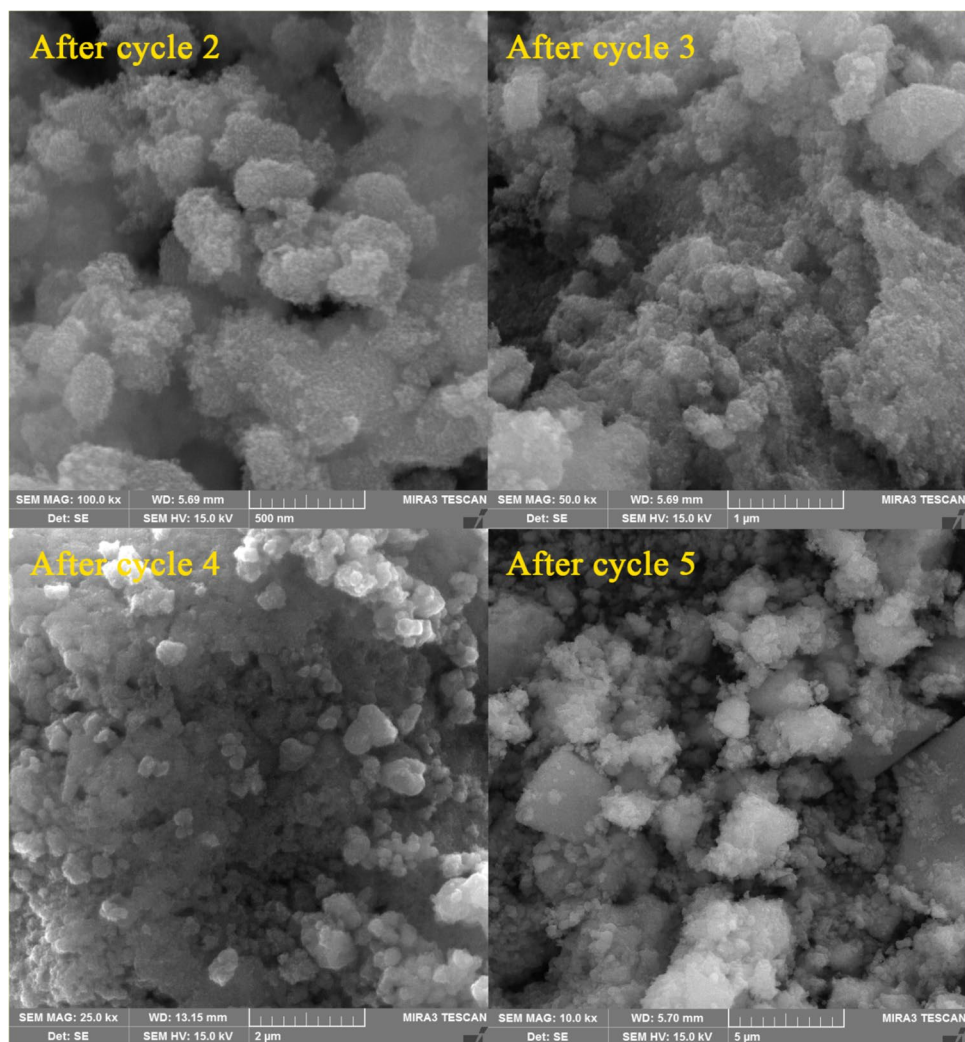


Stability of photocatalysts is an important criteria for practical applications (Yin et al. 2015). The 0.5Pt-CT sample was removed, washed, and dried for 5 h prior to use in five consecutive reaction cycles. As illustrated in Fig. 11, DBT removal efficiency decreased only slightly in consecutive cycles under visible-light exposure that could be attributed to the slight sintering of the catalyst as can be seen in Fig. 12.

## Conclusions

Photocatalysts were prepared by loading Pt on carbon-doped TiO<sub>2</sub> nanoparticles by a photo-deposition method for DBT photo-oxidation under visible-light illumination. Methanol was used as a polar solvent extractor. Ninety-eight percent of DBT removal was achieved in 3.5 h using the 0.5Pt-CT sample for an initial DBT concentration of 250 mg/l. Despite

**Fig. 12** FESEM images after consecutive reaction cycles over 0.5Pt-CT sample



5 cycles of repeated photocatalytic reactions, the catalyst only showed a slight decrease in activity.

**Supplementary Information** The online version contains supplementary material available at <https://doi.org/10.1007/s11356-023-26597-y>.

**Authors' contribution** Abdollah Ostovar: investigation, writing (original draft preparation). Afsanehsadat Larimi: project managing, supervision, conceptualization, methodology, funding acquisition. Zhi Jiang: conceptualization, methodology. Marzieh Lotfi, Farhad Khorasheh: writing (reviewing and editing).

**Funding** The authors gratefully acknowledge the support received from the Iran National Science Foundation (INSF) under the grant number 4001621.

**Data availability** All data generated or analyzed during this study are included in this published article.

## Declarations

**Ethics approval and consent to participate** Not applicable.

**Consent for publication** All listed authors have approved the manuscript before submission.

**Competing interests** The authors declare no competing interests.

## References

- Abdollahi M, Larimi A, Jiang Z, Khorasheh F, Ghotbi C (2022) Photocatalytic oxidative desulfurization of model fuel over visible light-active Cu-impregnated carbon-doped TiO<sub>2</sub>. *J Clean Prod* 380:134968. <https://doi.org/10.1016/j.jclepro.2022.134968>
- Anpo M, Kim TH, Matsuoka M (2009) The design of Ti-, V-, Cr-oxide single-site catalysts within zeolite frameworks and their photocatalytic reactivity for the decomposition of undesirable molecules—the role of their excited states and reaction mechanisms. *Catal Today* 142:114–124. <https://doi.org/10.1016/J.CATTOD.2008.11.006>
- Attar A, Corcoran WH (1978) Desulfurization of organic sulfur compounds by selective oxidation. 1. Regenerable and nonregenerable oxygen carriers. *Ind Eng Chem Prod Res Dev* 17:102–109. <https://doi.org/10.1021/i360066a003>
- Boonyasuwat S, Tscheikuna J (2017) Co-processing of palm fatty acid distillate and light gas oil in pilot-scale hydrodesulfurization unit over commercial CoMo/Al<sub>2</sub>O<sub>3</sub>. *Fuel* 199:115–124. <https://doi.org/10.1016/J.FUEL.2017.02.069>
- Campos-Martin JM, Capel-Sanchez MC, Perez-Presas P, Fierro JLG (2010) Oxidative processes of desulfurization of liquid fuels. *J Chem Technol Biotechnol* 85:879–890. <https://doi.org/10.1002/JCTB.2371>
- Chamack M, Ifires M, Akbar Razavi SA, Morsali A, Addad A, Larimi A, Szunerits S, Boukherroub R (2022) Photocatalytic performance of perovskite and metal–organic framework hybrid material for the reduction of N<sub>2</sub> to ammonia. *Inorg Chem* 61:1735–1744. <https://doi.org/10.1021/acs.inorgchem.1c03622>
- Chi J, Jiang Z, Yan J, Larimi A, Wang Z, Wang L, Shanguan W (2022) Recent advancements in bismuth vanadate photoanodes for photoelectrochemical water splitting. *Mater Today Chem* 26:101060. <https://doi.org/10.1016/J.MTCHEM.2022.101060>
- Choi H, Sofranko AC, Dionysiou DD (2006) Nanocrystalline TiO<sub>2</sub> Photocatalytic membranes with a hierarchical mesoporous multilayer structure: synthesis, characterization, and multifunction. *Adv Funct Mater* 16:1067–1074. <https://doi.org/10.1002/ADFM.200500658>
- Danish M, Tayyab M, Akhtar A, Altaf AA, Kausar S, Ullah S, Iqbal M (2021) Effect of soft template variation on the synthesis, physical, and electrochemical properties of Mn<sub>3</sub>O<sub>4</sub> nanomaterial. *Inorg Nano-Metal Chem* 51:359–365. <https://doi.org/10.1080/24701556.2020.1790000>
- Dong F, Guo S, Wang H, Li X, Wu Z (2011) Enhancement of the visible light photocatalytic activity of C-doped TiO<sub>2</sub> nanomaterials prepared by a green synthetic approach. *J Phys Chem C* 115:13285–13292. <https://doi.org/10.1021/jp111916q>
- Erdem B, Hunsicker RA, Simmons GW, Sudol ED, Dimonie VL, El-Aasser MS (2001) XPS and FTIR surface characterization of TiO<sub>2</sub> particles used in polymer encapsulation. *Langmuir* 17:2664–2669. <https://doi.org/10.1021/LA0015213>
- Giannakas AE, Antonopoulou M, Daikopoulos C, Deligiannakis Y, Konstantinou I (2016) Characterization and catalytic performance of B-doped, B–N co-doped and B–N–F tri-doped TiO<sub>2</sub> towards simultaneous Cr(VI) reduction and benzoic acid oxidation. *Appl Catal B Environ* 184:44–54. <https://doi.org/10.1016/J.APCATB.2015.11.009>
- Giannakas AE, Antonopoulou M, Papavasiliou J, Deligiannakis Y, Konstantinou I (2017) Photocatalytic performance of Pt–TiO<sub>2</sub>, Pt–N–TiO<sub>2</sub> and Pt–N/F–TiO<sub>2</sub> towards simultaneous Cr(VI) reduction/benzoic acid oxidation: insights into photogenerated charge carrier dynamics and catalyst properties. *J Photochem Photobiol A Chem* 349:25–35. <https://doi.org/10.1016/j.jphotochem.2017.08.066>
- Hitam CN, Jalil AA, Triwahyono S, Ahmad A, Jaafar NF, Salamun N, Fatah NA, Teh LP, Khusnun NF, Ghazali Z (2016) Synergistic interactions of Cu and N on surface altered amorphous TiO<sub>2</sub> nanoparticles for enhanced photocatalytic oxidative desulfurization of dibenzothiophene. *RSC Adv* 6:76259–76268. <https://doi.org/10.1039/C6RA06684D>
- Huang DG, Liao SJ, Zhou WB, Quan SQ, Liu L, He ZJ, Wan JB (2009) Synthesis of samarium- and nitrogen-co-doped TiO<sub>2</sub> by modified hydrothermal method and its photocatalytic performance for the degradation of 4-chlorophenol. *J Phys Chem Solids* 70:853–859. <https://doi.org/10.1016/J.JPCS.2009.04.005>
- Huang Y, Ho W, Lee S, Zhang L, Li G, Yu JC (2008) Effect of carbon doping on the mesoporous structure of nanocrystalline titanium dioxide and its solar-light-driven photocatalytic degradation of NO<sub>x</sub>. *Langmuir* 24:3510–3516. <https://doi.org/10.1021/LA703333Z>
- Huang Z, Song H, Li A, An Z, Zhang K, Xiang X, Shu X, He J (2020) Z-scheme ZnM-LDHs/g-C<sub>3</sub>N<sub>4</sub> (M = Al, Cr) photocatalysts: their desulfurization performance and mechanism for model oil with air. *Energy & Fuels* 34:14676–14687. <https://doi.org/10.1021/acs.energyfuels.0c02550>
- Ishibai Y, Sato J, Akita S, Nishikawa T, Miyagishi S (2007) Photocatalytic oxidation of NO<sub>x</sub> by Pt-modified TiO<sub>2</sub> under visible light irradiation. *J Photochem Photobiol A Chem* 188:106–111. <https://doi.org/10.1016/j.jphotochem.2006.11.026>
- Ismagilov ZR, Kerzhentsev MA, Yashnik SA, Khairulin SR, Salnikov AV, Parmon VN, Bourane A, Koseoglu OR (2015) New gas-phase catalytic oxidative processes for desulfurization of diesel fuel. *Eurasian Chem J* 17:119–128. <https://doi.org/10.18321/ECTJ202>
- Jaafar NF, Jalil AA, Triwahyono S, Efendi J, Mukti RR, Jusoh R, Jusoh NW, Karim AH, Salleh NF, Suendo V (2015) Direct in situ activation of Ag<sub>0</sub> nanoparticles in synthesis of Ag/TiO<sub>2</sub> and its photoactivity. *Appl Surf Sci* 338:75–84. <https://doi.org/10.1016/J.APSUSC.2015.02.106>
- Kalantari K, Kalbasi M, Sohrabi M, Royaei SJ (2016) Synthesis and characterization of N-doped TiO<sub>2</sub> nanoparticles and their application in photocatalytic oxidation of dibenzothiophene under visible

- light. *Ceram Int* 42:14834–14842. <https://doi.org/10.1016/j.ceramint.2016.06.117>
- Kalantari K, Kalbasi M, Sohrabi M, Royaei SJ (2017) Enhancing the photocatalytic oxidation of dibenzothiophene using visible light responsive Fe and N co-doped TiO<sub>2</sub> nanoparticles. *Ceram Int* 43:973–981. <https://doi.org/10.1016/j.ceramint.2016.10.028>
- Larimi A, Asgharinezhad A, Esmailpour M (2022) An overview on the use of metal-organic frameworks as photocatalysts for reducing carbon dioxide. *Iran Chem Eng J* 21(124):43–56. <https://doi.org/10.22034/ijche.2022.313360.1148>
- Larimi A, Khorasheh F (2020) Carbonaceous supports decorated with Pt–TiO<sub>2</sub> nanoparticles using electrostatic self-assembly method as a highly visible-light active photocatalyst for CO<sub>2</sub> photoreduction. *Renew Energy* 145:1862–1869. <https://doi.org/10.1016/j.renene.2019.07.105>
- Li FB, Li XZ (2002) The enhancement of photodegradation efficiency using Pt–TiO<sub>2</sub> catalyst. *Chemosphere* 48:1103–1111. [https://doi.org/10.1016/S0045-6535\(02\)00201-1](https://doi.org/10.1016/S0045-6535(02)00201-1)
- Li L, Huang X, Hu T et al (2014) Synthesis of three-dimensionally ordered macroporous composite Ag/Bi<sub>2</sub>O<sub>3</sub>–TiO<sub>2</sub> by dual templates and its photocatalytic activities for degradation of organic pollutants under multiple modes. *New J Chem* 38:5293–5302. <https://doi.org/10.1039/C4NJ01002G>
- Li S, Mominou N, Wang Z, Liu L, Wang L (2016) Ultra-deep desulfurization of gasoline with CuW/TiO<sub>2</sub>–GO through photocatalytic oxidation. *Energy & Fuels* 30:962–967. <https://doi.org/10.1021/acs.energyfuels.5b02790>
- Li X, Zhu W, Lu X, Zuo S, Yao C, Ni C (2017) Integrated nanostructures of CeO<sub>2</sub>/attapulgite/g-C<sub>3</sub>N<sub>4</sub> as efficient catalyst for photocatalytic desulfurization: mechanism, kinetics and influencing factors. *Chem Eng J* 326:87–98. <https://doi.org/10.1016/j.cej.2017.05.131>
- Lin YT, Weng CH, Lin YH, Shiesh CC, Chen FY (2013) Effect of C content and calcination temperature on the photocatalytic activity of C-doped TiO<sub>2</sub> catalyst. *Sep Purif Technol* 116:114–123. <https://doi.org/10.1016/j.seppur.2013.05.018>
- Liu G, Feng M, Tayyab M et al (2021) Direct and efficient reduction of perfluorooctanoic acid using bimetallic catalyst supported on carbon. *J Hazard Mater* 412:125224. <https://doi.org/10.1016/j.jhazmat.2021.125224>
- Liu G, Han C, Pelaez M, et al (2012) Synthesis, characterization and photocatalytic evaluation of visible light activated C-doped {TiO<sub>2</sub>}<sub>2</sub>nanoparticles. *Nanotechnology* 23:294003. <https://doi.org/10.1088/0957-4484/23/29/294003>
- Liu J, Zhang Q, Yang J, et al (2014) Facile synthesis of carbon-doped mesoporous anatase TiO<sub>2</sub> for the enhanced visible-light driven photocatalysis. *Chem Commun* 50:13971–13974. <https://doi.org/10.1039/C4CC05544F>
- Liu Y, Zhu Q, Tayyab M, Zhou L, Lei J, Zhang J (2021) Single-atom Pt loaded zinc vacancies ZnO–ZnS induced type-V electron transport for efficiency photocatalytic H<sub>2</sub> evolution. *Sol RRL* 5:2100536. <https://doi.org/10.1002/solr.202100536>
- Masoomi MY, Bagheri M, Morsali A (2015) Application of two cobalt-based metal-organic frameworks as oxidative desulfurization catalysts. *Inorg Chem* 54:11269–11275. [https://doi.org/10.1021/ACS.INORGCHEM.5B01850/SUPPL\\_FILE/IC5B01850\\_SI\\_001.PDF](https://doi.org/10.1021/ACS.INORGCHEM.5B01850/SUPPL_FILE/IC5B01850_SI_001.PDF)
- McManamon C, O'Connell J, Delaney P, Rasappa S, Holmes JD, Morris MA (2015) A facile route to synthesis of S-doped TiO<sub>2</sub> nanoparticles for photocatalytic activity. *J Mol Catal A Chem* 406:51–57. <https://doi.org/10.1016/J.MOLCATA.2015.05.002>
- Moradi M, Khorasheh F, Larimi A (2020) Pt nanoparticles decorated Bi-doped TiO<sub>2</sub> as an efficient photocatalyst for CO<sub>2</sub> photo-reduction into CH<sub>4</sub>. *Sol Energy* 211:100–110. <https://doi.org/10.1016/j.solener.2020.09.054>
- Moradi M, Khorasheh F, Larimi A, Nematollahi R (2019) Photo-assisted deposition of Pt nanoparticles onto TiO<sub>2</sub> as highly active nano- photocatalyst for CO<sub>2</sub> photoreduction, pp 20–22
- Moradi M, Larimi A, Khorasheh F, Nematollahi R (2020) Photocatalytic reduction of carbon dioxide to renewable methane using titanium dioxide modified with bismuth and copper. *mdrsjrns* 4:43–55
- Moradi S, Vossoughi M, Feilizadeh M, Zakeri SM, Mohammadi MM, Rashtchian D, Yoosefi Booshehri A (2015) Photocatalytic degradation of dibenzothiophene using La/PEG-modified TiO<sub>2</sub> under visible light irradiation. *Res Chem Intermed* 41:4151–4167. <https://doi.org/10.1007/s11164-013-1519-z>
- Moradi V, Jun MBG, Blackburn A, Herring RA (2018) Significant improvement in visible light photocatalytic activity of Fe doped TiO<sub>2</sub> using an acid treatment process. *Appl Surf Sci* 427:791–799. <https://doi.org/10.1016/J.APSUSC.2017.09.017>
- Mousavi-Kamazani M, Ashrafi S (2020) Single-step sonochemical synthesis of Cu<sub>2</sub>O–CeO<sub>2</sub> nanocomposites with enhanced photocatalytic oxidative desulfurization. *Ultrason Sonochem* 63:104948. <https://doi.org/10.1016/j.ultsonch.2019.104948>
- Nasirian Bachelor M (2021) Development of a novel photocatalyst for the photocatalytic treatment of industrial wastewater. <https://doi.org/10.32920/RYERSON.14647518.V1>
- Nematollahi R, Ghotbi C, Khorasheh F, Larimi A (2020) Ni–Bi co-doped TiO<sub>2</sub> as highly visible light response nano-photocatalyst for CO<sub>2</sub> photo-reduction in a batch photo-reactor. *J CO<sub>2</sub> Util* 41:101289. <https://doi.org/10.1016/j.jcou.2020.101289>
- Nematollahi R, Ghotbi C, Khorasheh F, et al (2019) Sol-gel derived bismuth modified TiO<sub>2</sub>, a highly visible light response nano-photocatalyst for CO<sub>2</sub> photoreduction. 20–22
- Nematollahi R, Larimi A, Ghotbi C, Khorasheh F, Moradi M (2021) Methane production by CO<sub>2</sub> photo-reduction in the presence of TiO<sub>2</sub> modified by nickel and copper. *Appl Chem* 16:37–48. <https://doi.org/10.22075/chem.2021.19404.1776>
- Ochoa Rodríguez PA, Benzaquén TB, Pecchi GA, Casuscelli SG, Elías VR, Eimer GA (2019) Novel route to obtain carbon self-doped TiO<sub>2</sub> mesoporous nanoparticles as efficient photocatalysts for environmental remediation processes under visible light. *Mater* 12(20):3349
- Peng F, Gao H, Zhang G, Zhu Z, Zhang J, Liu Q (2017) Synergistic effects of Sm and C Co-doped mixed phase crystalline TiO<sub>2</sub> for visible light photocatalytic activity. *Mater* 10:209. <https://doi.org/10.3390/MA10020209>
- Pham XN, Nguyen MB, Ngo HS, Doan HV (2020) Highly efficient photocatalytic oxidative desulfurization of dibenzothiophene with sunlight irradiation using green catalyst of Ag@AgBr/Al-SBA-15 derived from natural halloysite. *J Ind Eng Chem* 90:358–370. <https://doi.org/10.1016/j.jiec.2020.07.037>
- Pillai S, Pelaez M, Kontosd AG (2012) A review on the visible light active titanium dioxide photocatalysts for.pdf., vol 125, pp 331–349
- Samsudin EM, Abd Hamid SB, Juan JC, Basirun WJ, Centi G (2016) Synergetic effects in novel hydrogenated F-doped TiO<sub>2</sub> photocatalysts. *Appl Surf Sci* 370:380–393. <https://doi.org/10.1016/J.APSUSC.2016.02.172>
- Shang H, Guo C, Ye P, Zhang W (2020) Synthesis of boron modified CoMo/Al<sub>2</sub>O<sub>3</sub> catalyst under different heating methods and its gasoline hydrodesulfurization performance. *Front Chem Sci Eng* 155(15):1088–1098. <https://doi.org/10.1007/S11705-020-1969-Y>
- Shu Z, Cai Y, Ji J, Tang C, Yu S, Zou W, Dong L (2020) Pt deposits on TiO<sub>2</sub> for photocatalytic H<sub>2</sub> evolution: Pt is not only the cocatalyst, but also the defect repair agent. *Catalysts* 10(9):1047. <https://doi.org/10.3390/catal10091047>

- Song C (2003) An overview of new approaches to deep desulfurization for ultra-clean gasoline, diesel fuel and jet fuel. *Catal Today* 86:211–263. [https://doi.org/10.1016/S0920-5861\(03\)00412-7](https://doi.org/10.1016/S0920-5861(03)00412-7)
- Song H, You JA, Li B, Chen C, Huang J, Zhang J (2017) Synthesis, characterization and adsorptive denitrogenation performance of bimodal mesoporous Ti-HMS/KIL-2 composite: a comparative study on synthetic methodology. *Chem Eng J* 327:406–417. <https://doi.org/10.1016/J.CEJ.2017.06.055>
- Sood S, Umar A, Mehta SK, Kansal SK (2015) Highly effective Fe-doped TiO<sub>2</sub> nanoparticles photocatalysts for visible-light driven photocatalytic degradation of toxic organic compounds. *J Colloid Interface Sci* 450:213–223. <https://doi.org/10.1016/j.jcis.2015.03.018>
- Stevanovic A, Büttner M, Zhang Z, Yates JT (2011) Photoluminescence of TiO<sub>2</sub>: effect of UV light and adsorbed molecules on surface band structure. *J Am Chem Soc* 134:324–332. <https://doi.org/10.1021/JA2072737>
- Tayyab M, Liu Y, Liu Z, Pan L, Xu Z, Yue W, Zhou L, Lei J, Zhang J (2022) One-pot in-situ hydrothermal synthesis of ternary In<sub>2</sub>S<sub>3</sub>/Nb<sub>2</sub>O<sub>5</sub>/Nb<sub>2</sub>C Schottky/S-scheme integrated heterojunction for efficient photocatalytic hydrogen production. *J Colloid Interface Sci* 628:500–512. <https://doi.org/10.1016/j.jcis.2022.08.071>
- Tayyab M, Liu Y, Min S, Irfan RM, Zhu Q, Zhou L, Lei J, Zhang J (2022) Simultaneous hydrogen production with the selective oxidation of benzyl alcohol to benzaldehyde by a noble-metal-free photocatalyst VC/CdS nanowires. *Chinese J Catal* 43:1165–1175. [https://doi.org/10.1016/S1872-2067\(21\)63997-9](https://doi.org/10.1016/S1872-2067(21)63997-9)
- Wang C, Zhu W, Xu Y, Xu H, Zhang M, Chao Y, Yin S, Li H, Wang J (2014) Preparation of TiO<sub>2</sub>/g-C<sub>3</sub>N<sub>4</sub> composites and their application in photocatalytic oxidative desulfurization. *Ceram Int* 40:11627–11635. <https://doi.org/10.1016/j.ceramint.2014.03.156>
- Wang X, Tang Y, Leiw M-Y, Lim T-T (2011) Solvothermal synthesis of Fe–C codoped TiO<sub>2</sub> nanoparticles for visible-light photocatalytic removal of emerging organic contaminants in water. *Appl Catal A Gen* 409–410:257–266. <https://doi.org/10.1016/j.apcata.2011.10.011>
- Xie H, Li Y, Jin S, Han J, Zhao X (2010) Facile fabrication of 3D-ordered macroporous nanocrystalline iron oxide films with highly efficient visible light induced photocatalytic activity. *J Phys Chem C* 114:9706–9712. <https://doi.org/10.1021/jp102525y>
- Yaghoot-Nezhad A, Moradi M, Rostami M, Danaee I, Khosravi-Nikou MR (2020) Dual Z-scheme CuO-ZnO@graphitic carbon nitride ternary nanocomposite with improved visible light-induced catalytic activity for ultrasound-assisted photocatalytic desulfurization. *Energy & Fuels* 34:13588–13605. <https://doi.org/10.1021/acs.energyfuels.0c02012>
- Yin H, Wang X, Wang L, Lin N, Zhao H (2015) Self-doped TiO<sub>2</sub> hierarchical hollow spheres with enhanced visible-light photocatalytic activity. *J Alloys Compd* 640:68–74. <https://doi.org/10.1016/J.JALLCOM.2015.03.216>
- Yu J, Dai G, Xiang Q, Jaroniec M (2011) Fabrication and enhanced visible-light photocatalytic activity of carbon self-doped TiO<sub>2</sub> sheets with exposed {001} facets. *J Mater Chem* 21:1049–1057. <https://doi.org/10.1039/C0JM02217A>
- Zhang M, Zhu W, Xun S, Li H, Gu Q, Zhao Z, Wang Q (2013) Deep oxidative desulfurization of dibenzothiophene with POM-based hybrid materials in ionic liquids. *Chem Eng J* 220:328–336. <https://doi.org/10.1016/J.CEJ.2012.11.138>
- Zhang X, Huang P, Liu A, Zhu M (2017) A metal–organic framework for oxidative desulfurization: UIO-66(Zr) as a catalyst. *Fuel* 209:417–423. <https://doi.org/10.1016/J.FUEL.2017.08.025>

**Publisher's note** Springer Nature remains neutral with regard to jurisdictional claims in published maps and institutional affiliations.

Springer Nature or its licensor (e.g. a society or other partner) holds exclusive rights to this article under a publishing agreement with the author(s) or other rightsholder(s); author self-archiving of the accepted manuscript version of this article is solely governed by the terms of such publishing agreement and applicable law.